CdSe/CdS/CdTe Core/Barrier/Crown Nanoplatelets: Synthesis, Optoelectronic Properties and Multi-Photon Fluorescence Upconversion - Supporting Information

Ali Hossain Khan,[1,2] Guillaume H. V. Bertrand,[2] Ayelet Teitelboim,[3] Chandra Sekhar M.,[1] Anatolii Polovitsyn,[2] Rosaria Brescia,[2] Josep Planelles,[4] Juan Ignacio Climente,[4,] Dan Oron,[3,*] and Iwan Moreels[1,2,*]*

[1] Department of Chemistry, Ghent University, Krijgslaan 281-S3, 9000 Ghent, Belgium.

[2] Istituto Italiano di Tecnologia, Via Morego 30, 16163 Genova, Italy.

[3] Department of Physics of Complex Systems, Weizmann Institute of Science, Rehovot 7610001, Israel.

[4] Departament de Química Física i Analítica, Universitat Jaume I, 12080 Castelló de la Plana, Spain.

Present Addresses

Guillaume H. V. Bertrand: CEA Saclay, 91191 Gif-sur-Yvette, France

Ayelet Teitelboim: The Molecular Foundry, Lawrence Berkeley National Laboratory, Berkeley, California 94720, United States

1. ADDITIONAL ABSORPTION, PHOTOLUMINESCENCE AND TEM DATA

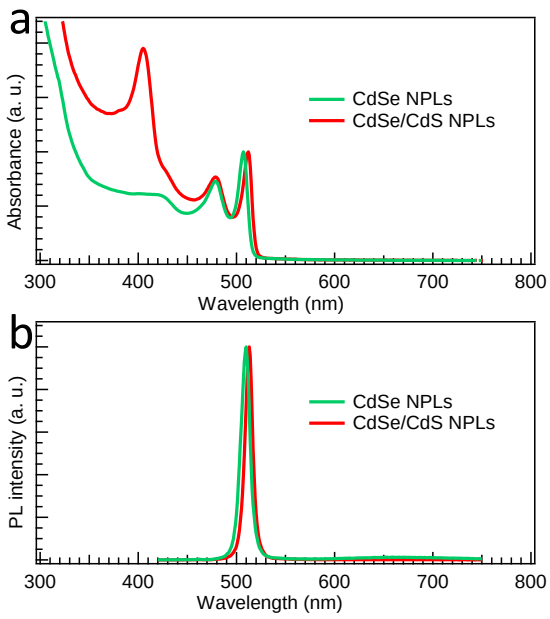

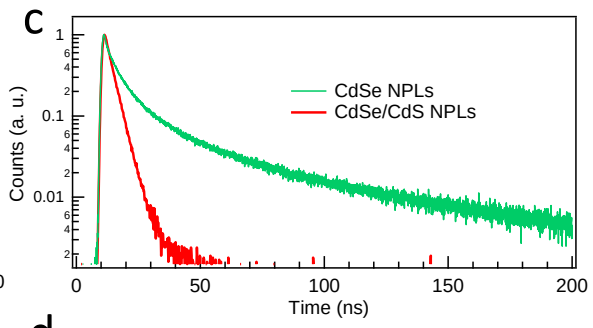

d

Sample name	Abs_{max} (nm)	PL_{max} (nm)	τ_{av} (ns)
CdSe NPLs	507	510	8.2
CdSe/CdS NPLs	511	513	3.3

Figure S1. (a) Absorption spectra, (b) PL spectra and (c) PL decay traces of CdSe core (green) and CdSe/CdS core/crown (red) NPLs. For the latter, samples were excited at 331 nm with a pulsed LED. (d) Table containing the value of absorption and PL peak maximum and the amplitude-weighted average lifetime of CdSe core and CdSe/CdS core/crown NPLs.

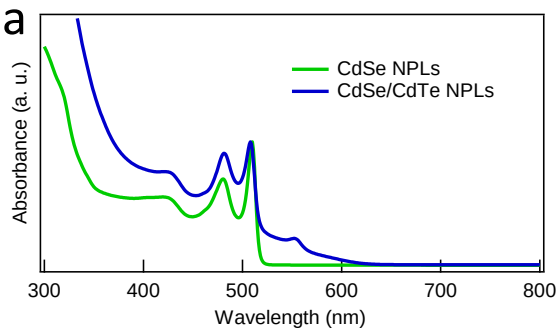

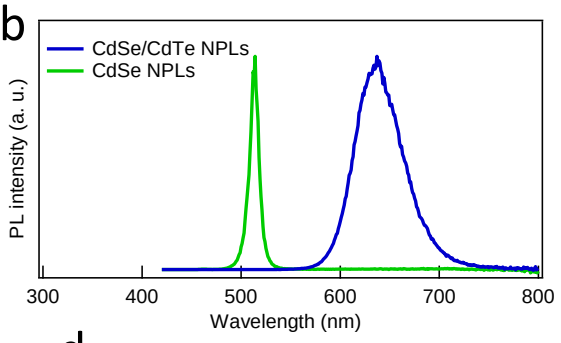

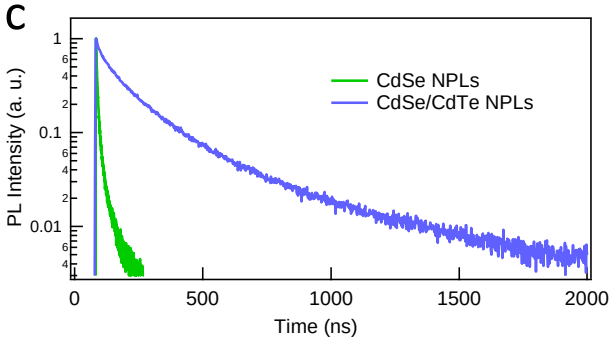

d

Sample name	PL_{max} (nm)	τ_{av} (ns)
CdSe NPLs	513	6.2
CdSe/CdTe NPLs	637	124

Figure S2. (a) Absorption spectra, (b) PL spectra and (c) PL decay traces of CdSe core and CdSe/CdTe core/crown NPLs. For the latter, samples were excited at 405 nm. (d) Table containing the value of absorption and PL peak maximum and the amplitude-weighted average lifetime of CdSe core and CdSe/CdTe core/crown NPLs.

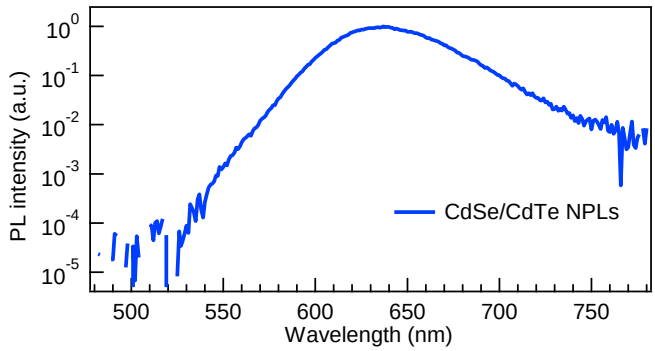

Fit name	Emission of	Peak location (nm)	FWHM (nm)	Area %
Peak 1	CdSe	514	7.0	0.001
Peak 2	type-II	637	59.7	99.996

Figure S3. PL spectrum of CdSe/CdTe core/crown NPLs. The emission from the CdSe direct transition is negligible. The table is the summary of the peak fitting results.

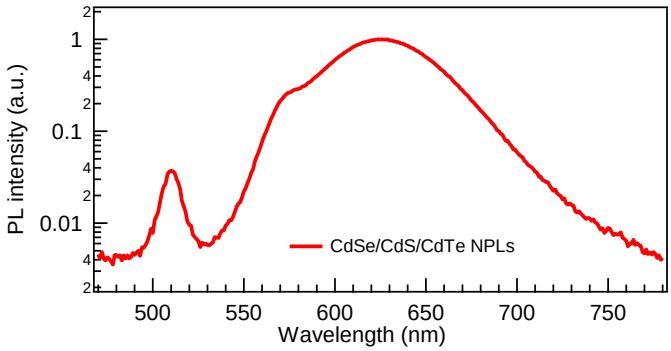

	Emission	Peak location (nm)	FWHM (nm)	Area (%)
Peak 1	CdSe	510	11.1	0.5
Peak 2	CdTe	574	21.0	4.2
Peak 3	type-II	625	58.8	95.3

Figure S4. PL spectrum of CdSe/CdS/CdTe CBC NPLs. In contrast with CdSe/CdTe NPLs, clear features for the CdSe and CdTe direct transitions are observed. The table is the summary of the peak fitting results.

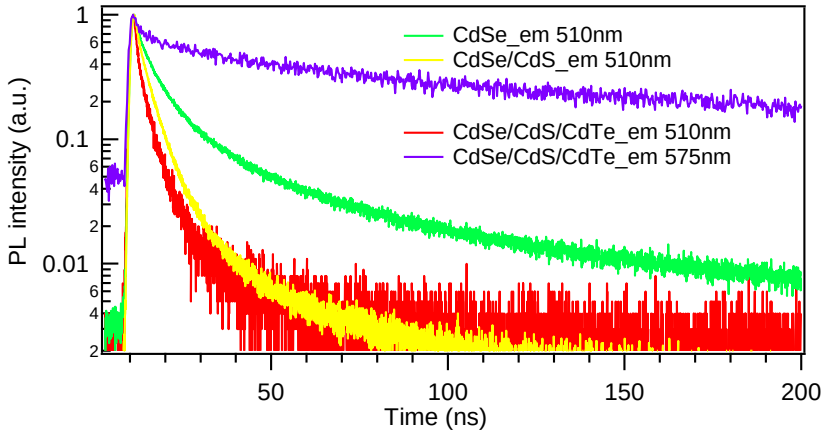

Name	A_1	τ_1	A_2	τ_2	A_3	τ_3	τ_{av} (ns)
CdSe@510	0.32	1.4	0.57	6.3	0.13	33.6	8.2
CB@510	0.43	1.6	0.59	4.6	0.03	25.1	3.9
CBC@510	0.70	1.2	0.37	4.4	0.01	30.1	2.6
CBC@575	0.38	2.9	0.31	39.4	0.26	225.2	76
CBC@625	0.24	15.6	0.47	122	0.22	481	182

Figure S5. Upper panel: PL decay traces of CdSe core (green) CdSe/CdS (yellow), and CBC (red and purple) NPLs (Batch3) at different emission wavelength. Lower panel: Table containing the decay amplitudes and lifetimes, and the amplitude-weighted average lifetime of the different NPLs.

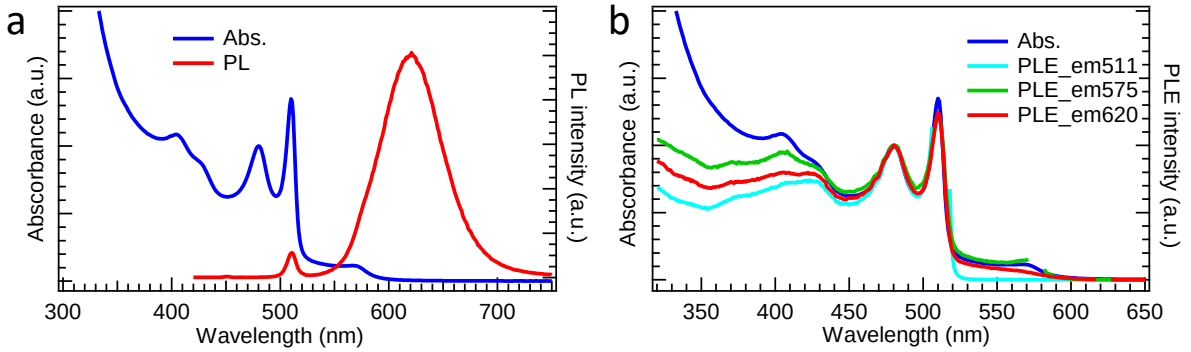

Figure S6. (a) Absorption and PL of the CBC NPLs with wider CdS barrier (Batch5). (b) PLE spectra of CBC NPLs at different emission wavelengths.

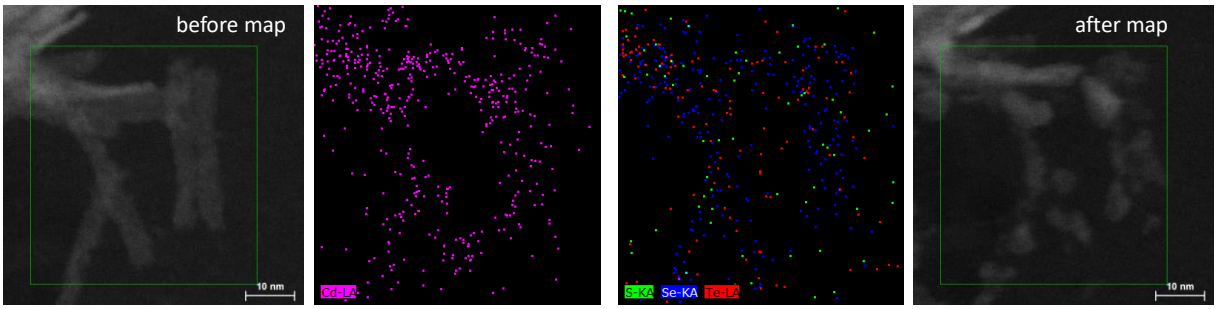

Figure S7. HAADF-STEM images (leftmost and rightmost) of CBC NPLs (Batch3) showing the degradation of the NPL structure after 19 minutes of acquisition of STEM-EDS elemental maps (using a 1 nm spot size). The acquired elemental maps for Cd, S, Se and Te are shown in the central panels.

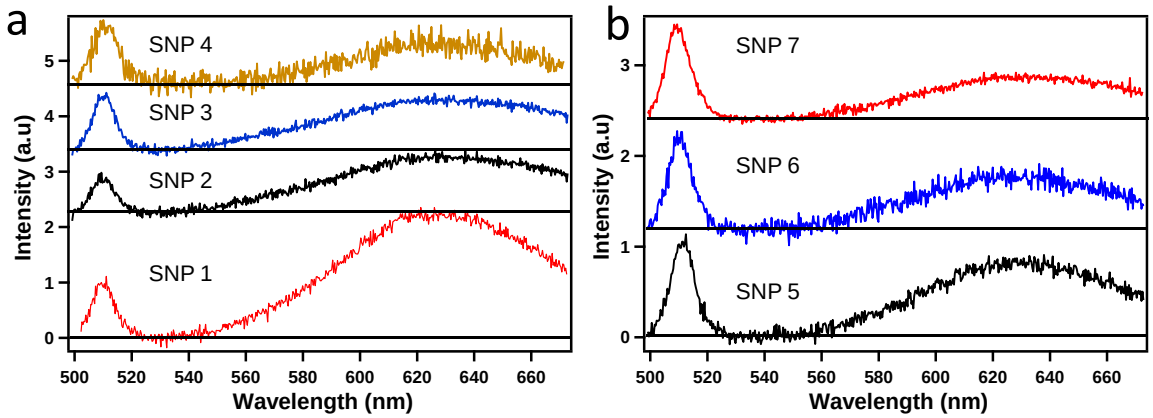

Figure S8. (a-b) PL spectra of various single CBC NPLs, showing the presence of both CdSe and type-II emission. For single particle PL measurement batch 5 CBC NPLs have been used, which had PL quantum efficiency of 15%.

Table S1: The peak position and FWHM of CdSe and type II emission of various single NPLs and corresponding close-packed thin film.

CdSe/CdS/CdTe (CBC) NPLs	Type I		Type II	
	Peak Maximum (nm)	FWHM (nm)	Peak Maximum (nm)	FWHM (nm)
Film	511.9	13.6	631.4	81.7
SNP 1	510.0	10.8	629.9	88.2
SNP 2	509.9	10.9	632.8	106.1
SNP 3	510.3	10.2	632.2	109.6
SNP 4	510.9	10.7	629.2	74.8
SNP 5	511.5	10.6	631.3	80.6
SNP 6	510.4	10.9	629.5	87.4
SNP 7	509.8	11.2	633.8	90.3

Table S2. The dimensions (obtained from TEM) of CdS barrier and CdTe crown achieved by injecting different amounts of Cd/S and Te growth solutions. The injection rate of the precursor solution was always kept at a fixed rate of 3 mL per hour. For some samples, negative values were be obtained when initial and final particle dimensions were similar, indicating a negligible CdS barrier and/or CdTe crown growth.

	Core	**Core/Barrier**		**Core/Barrier/Crown**	
Name	Length × Width (nm x nm)	CdS solution injection rate (min)	CdS Barrier length × width (nm x nm)	Te solution injection rate (min)	CdTe crown length × width (nm x nm)
Batch1	31.1 x 6.4	2 min	-0.05 × 0.4	1 min	0.8 × -0.1
Batch2	30.3 x 6.4	4 min	0.6 × 1.1	4 min	2.5 × 0.4
Batch3	35.6 x 4.2	2 min	0.9 × 0.7	3 min	7.1 × 1.8
Batch4	24.3 x 5.0	12 min	8.8 × 2.3	16 min	7.5 × 2.9
Batch5	40.5 × 5.1	3 min	2.0 × 0.8	2 min	2.6 × 0.8

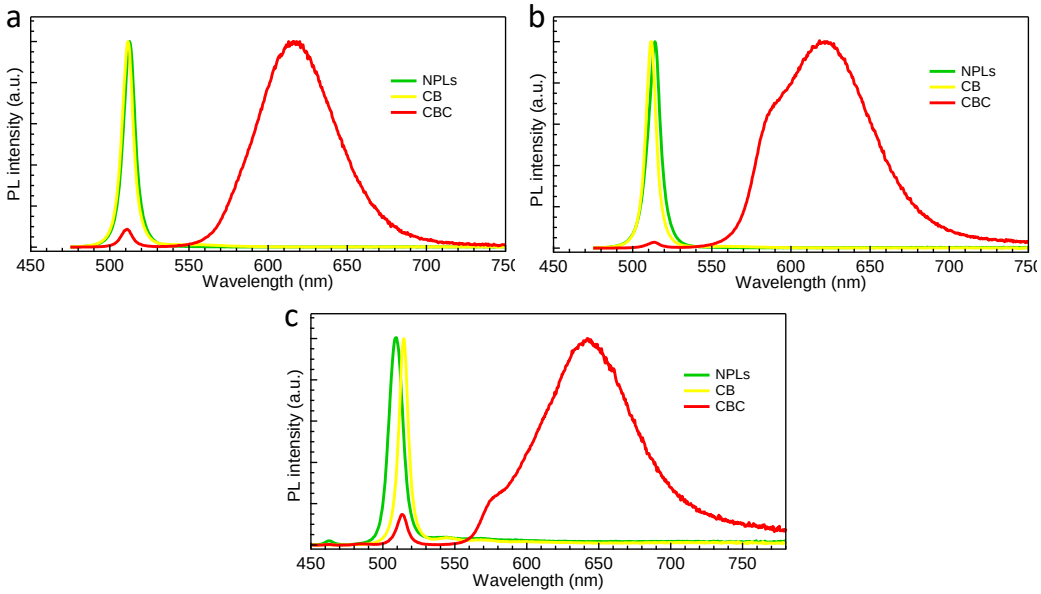

	Area CdSe (%)	Area CdTe (%)	Area type-II (%)
Batch1	1.3	0.8	97.8
Batch2	0.5	6.7	92.8
Batch4	1.8	2.8	95.4

Figure S9. PL spectra for core, core/barrier and core/barrier/crown samples of (a) Batch1 (narrow barrier), (b) Batch2 (medium barrier) and (c) Batch4 (wide barrier, bottom). Next to the indirect transitions, two additional features are observed that can be assigned to CdSe and CdTe emission. Relative weights are reported in the table. PL spectra of Batch3 are presented in Figure S4 and Figure 2 of the main text.

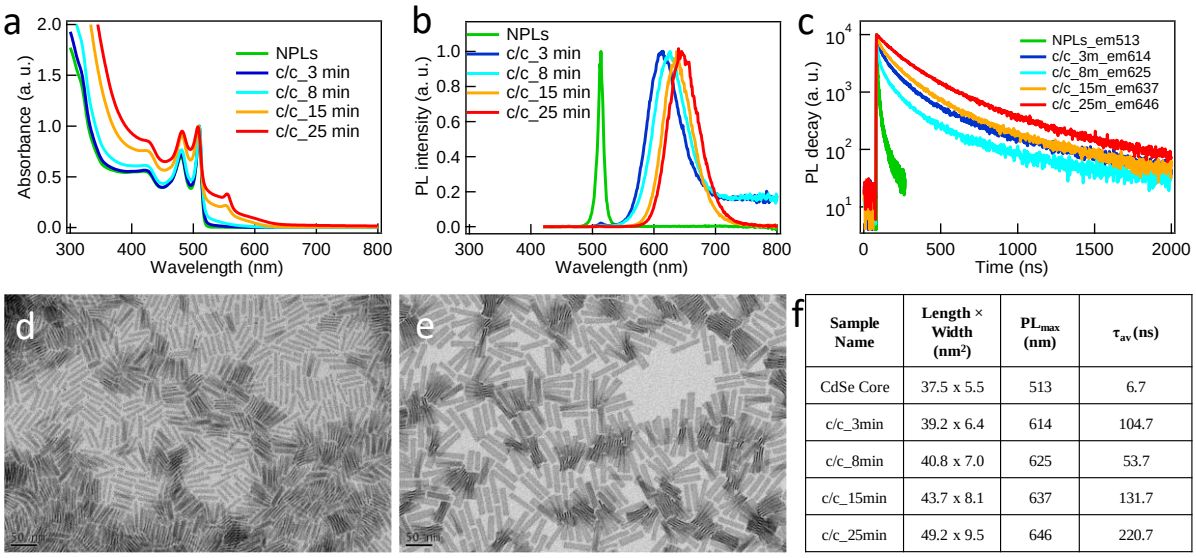

f

Sample Name	Length × Width (nm²)	PL_{max} (nm)	τ_{av} (ns)
CdSe Core	37.5 x 5.5	513	6.7
c/c_3min	39.2 x 6.4	614	104.7
c/c_8min	40.8 x 7.0	625	53.7
c/c_15min	43.7 x 8.1	637	131.7
c/c_25min	49.2 x 9.5	646	220.7

Figure S10. (a) Absorption spectra, (b) PL spectra and (c) PL decay traces of CdSe core and different CdSe/CdTe core/crown NPLs respectively. TEM images of (d) CdSe core and (e) CdSe/CdTe core/crown (sample c/c_25 min) NPLs. (f) Table containing the dimensions, value of PL peak maximum and the amplitude-weighted average lifetime of CdSe core and different CdSe/CdTe core/crown NPLs.

Table S3. Table with the PL peak position and amplitude-weighted average lifetime of the core, core/barrier and core/barrier/crown NPLs.

	core		**core/barrier**		**core/barrier/crown**		
	PL_core	τ_core	PL_core	τ_core	PL_core	PL_typeII	τ_typeII
Batch1	512	5.5	511	5.0	511	617	160
Batch2	512	5.8	513	4.2	513	621	157
Batch3	510	8.2	510	3.9	510	625	182
Batch4	509	4.0	513	2.7	513	642	182

2. THEORETICAL MODELING

Purpose and Method

To better understand the optoelectronic properties of CdSe/CdS/CdTe CBC NPLs, we carried out numerical simulations of the conduction band electrons and valence band (heavy) holes.

In view of the picture sketched in the main text, hole states are calculated using the Hamiltonian:

$$H_h = \frac{1}{2}\,\hat{p}\,\frac{1}{m_h(\vec{r})}\,\hat{p} + V_{self} + V_{bo}^{h} + V_{strain}^{h}\,.$$

Here m_h is the (position dependent) hole effective mass, p the three-dimensional momentum operator, V_{self} the self-energy potential arising from the dielectric mismatch between the inorganic NPL and the organic surroundings –which we calculate taking analytical quantum well expressions[1], V_{bo}^{h} is the (squared-well) valence band offset potential and V_{strain}^{h} the deformation potential strain Hamiltonian:

$$V_{strain}^{h} = \left(a_v + \frac{b}{2}\right)\left(\epsilon_{xx} + \epsilon_{yy}\right) + \left(a_v - b\right)\epsilon_{zz}\,,$$

with a_v and b the valence band deformation potentials, and ϵ_{ij} a strain tensor component.

For the electron, the full Hamiltonian reads:

$$H_e = \frac{1}{2}\,\hat{p}\,\frac{1}{m_e(\vec{r})}\,\hat{p} + V_{self} + V_{bo}^{e} + V_{strain}^{e} + V_{coul}^{e},$$

where m_e is the electron effective mass, V_{bo}^{e} is the conduction band offset potential, V_{strain}^{e} the deformation potential strain Hamiltonian:

$$V_{strain}^{e} = a_c\left(\epsilon_{xx} + \epsilon_{yy} + \epsilon_{zz}\right),$$

with a_c the conduction band deformation potential, and V_{coul}^{e} the Coulomb attraction exerted by the hole ground state (localized in the CdTe crown) on the electron, which includes the enhancement due to the low dielectric constant of the NPL surroundings.

Strain maps are calculated in the continuous medium model by minimizing the elastic energy. The boundary conditions are zero normal stress for the free surface. The Coulomb potential is obtained by solving Poisson's equation with the hole ground state as the source electric charge. Strain tensor elements, Coulomb electrostatic potential and eigenfunctions of H_e and H_h are obtained using Comsol 4.2 software. The calculations are simplified by imposing D_{2h} symmetry planes to the rectangular NPL, which allows us to identify electron and hole eigenstates by their point group symmetry. Thus, we label states as $|\Gamma, n\rangle$, which is the n-th state of the Γ irreducible representation. Material parameters used for the calculations are summarized in **Table S3**. Also, band offsets between bulk semiconductor materials are given in **Figure 4** of the main text.

Table S4. Summary of material parameters used in the calculation. m_0 is the free electron mass. The relative dielectric constant outside the NPL is 2 and the electron (hole) band offset with the organic medium 2.5 eV from the bottom (top) of the conduction (valence) band of CdSe. Band offsets are taken from Ref. 2, deformation potentials a_c and a_v are taken from Ref. 3, relative dielectric constant are approximate values between static and high-frequency dielectric constants, CdSe hole masses are taken from Ref. 4, and the rest of parameters from Ref. 5.

Parameter	**CdSe**	**CdS**	**CdTe**	**Parameter**	**CdSe**	**CdS**	**CdTe**
m_e^z (m_0)	0.11	0.14	0.09	m_h^z (m_0)	1.14	0.39	0.53
m_e^{xy} (m_0)	0.11	0.14	0.09	m_h^{xy} (m_0)	0.38	0.20	0.14
a_c (eV)	-2.00	-2.54	-2.81	a_v / b (eV)	0.9/-0.8	0.4/-1.05	0.89/-1.0
$C11$ (GPa)	66.7	77	53.5	ε_r	10	10	10
$C12$ (GPa)	46.3	53.9	36.9	a (Å)	6.077	5.825	6.481
$C44$ (GPa)	22.3	23.6	20.2				

Results and Discussion

We first analyzed the influence of the CdS barrier on the elastic strain. CdS has a strong lattice mismatch (over 10%) with CdTe, which is expected to alter the CdS/CdTe interface. **Figure S11** shows the hydrostatic strain in the wide (a) and narrow (b) barrier CBC NPLs (same as in **Figure 4** of the main text). As can be seen, most of the strain concentrates on the CdS barrier and –especially- on the first nm around the CdS/CdTe interface. By contrast, the center of the CdSe core and the outer part of the CdTe crown are only weakly affected.

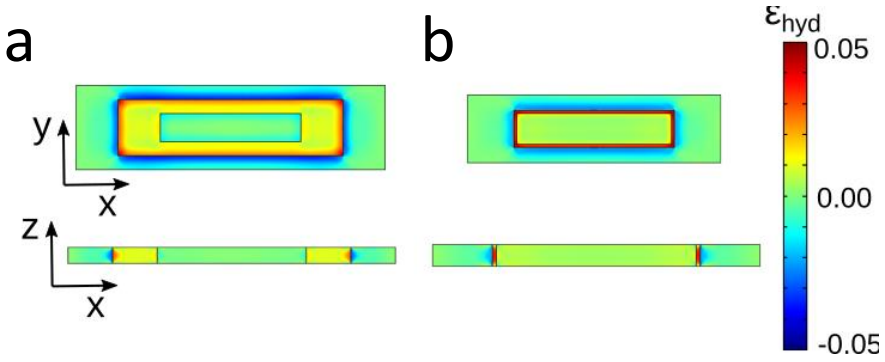

Figure S11. Hydrostatic strain $(\epsilon_{xx} + \epsilon_{yy} + \epsilon_{zz})$ in (a) wide and (b) narrow CdS barrier NPLs. The top (bottom) panels show an in-plane (vertical) section of the NPLs. Positive and negative strain are tensile and compressive, respectively.

The strain is tensile on the CdS side and compressive on the CdTe one. Considering the sign of the deformation potentials (**Table S4**), this means that a strain-induced potential well (barrier) forms on the CdS (CdTe) side of the barrier-crown interface, as seen in **Figure 4i-4j** of the main text.

The band profile of a typical wide barrier CBC NPL is shown in **Figure S12**. The figure completes the data of **Figure 4f-4j** of the main text for the wide CdS barrier NPL. Left and right columns show the potential corresponding to valence band (left) and conduction band (right). The top graphs are a 2D map of the potential on the (*x*,*y*) plane at mid-height. The central panels are 1D profiles along the *x*- semi-axis (as in **Figure 4f-4j**) and the bottom ones along the *y*-semi-axis. The role of band-offset and strain described in the main text holds all over the NPL plane. The Coulomb potential that the hole exerts on the electron (blue line) is more attractive at the CdS/CdTe interface along the *x*-axis than at the interface along the *y*-axis (cf. **Figure S12e-S12f**). This is because the narrow CdTe crown in the *y*-direction prevents a buildup of significant charge density in that region. The self-energy potential provides a constant shift all over the structure, which does not modify the relative band alignment.

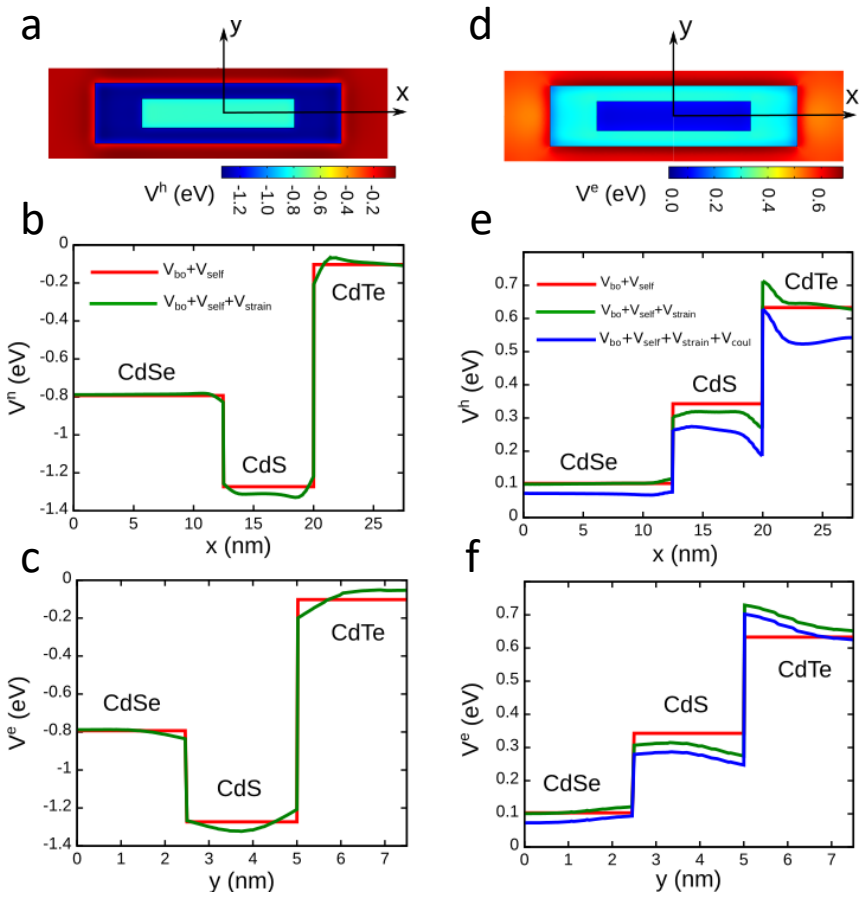

Figure S12. Potential landscape seen by a valence band hole (left) and a conduction band electron (right) in wide-barrier CBC NPLs. Top panels show a 2D in-plane cross-section (for *z* in the center of the NPL), while mid and bottom panels show the 1D profile along *x*- and *y*-semi-axes. In the 1D plots, red and green lines show the potential excluding and including the influence of strain, respectively. For electrons, we add Coulomb interaction with the hole ground state (blue line) to obtain the highest possible barrier at the CdS/CdTe interface.

The band structure shown in **Figure S12** gives rise to preferential localization of electron and –especially– hole states either in the core or in the crown, as discussed in **Figure 5** of the main text. This can be expected to affect the intraband transition rates from crown to core states, facilitating the formation of meta-stable states. The precise value of transition rates depends on the nature of the process (phononic, photonic, Auger, etc), however, quantitative calculations are beyond the scope of this paper. Assuming phonon decay is involved, as is often the case in colloidal quantum dots, the high surface-to-volume ratio of NPLs implies that confined, surface and interface phonon modes are expected to play a role.[6,7] These are not well described in continuum models like $k \cdot p$ theory. In any case, every scattering mechanism involves coupling the initial and final electronic states. If these are spatially separated, the scattering becomes less efficient.

For illustration purposes, we calculated transition dipole matrix elements, which are relevant to both photonic and phononic intraband processes. We considered that the lowest energy electron or hole states are *s*-like, *i.e.* they form a basis of the A_g irreducible representation in the D_{2h} group. In turn, *x*-, *y*- and *z*-coordinate operators form the basis of the B_{3u}, B_{2u} and B_{1u} irreducible representations. Then, the selection rule implies that the final state *f* should have B_{3u}, B_{2u} and B_{1u} symmetry, for *x*-, *y*- and *z*-components of the photon/phonon wave expansion. The largest dipole moments are expected along the *x*-direction (the long axis of the NPL). Then, we compute matrix elements of the kind $\langle B_{3u}, n' | x | A_g, n \rangle$ to evaluate $|\langle f | \vec{r} | i \rangle|$.

We considered as the initial state *i* the lowest hole (electron) state localized in CdSe (CdTe), and then computed the matrix element to all lower-energy states, to see if the respective CdSe-localized hole or CdTe-localized electron state has limited overlap with lower-lying states and is thus long-lived. The results are summarized in **Figure S13**. Panels (a) and (b) show the dipole matrix elements for hole transitions from the CdSe-localized state to all lower energy states, which are mainly localized in CdTe. One can see the matrix element is orders of magnitude smaller in wide-barrier NPLs (panel (a)) than in narrow ones (panel (b)). This is because the strong localization either in the core or in the crown makes the overlap between initial and final states negligible. This finding supports the formation of meta-stable hole states in the core, especially in samples with a wide barrier, which may recombine with electrons radiatively before non-radiative relaxation takes place.

Panels (c) and (d) show the matrix elements for electron transitions from the CdTe crown to CdSe core localized states. One can notice that the dipole moment is much larger than in the case of holes. This is because electrons show partial localization on both sides of the CdS barrier, which implies that relaxation of electrons should be much faster than for holes. The thickness of the barrier does make a large difference in the average rates. However, in accordance with experimental observations, narrowing the crown width (panels (e) and (f)) does provide an additional suppression of the dipole matrix elements. This is a consequence of the reduced electron localization on the short sides of the NPL, as mentioned in the discussion of **Figure 5** in the main text.

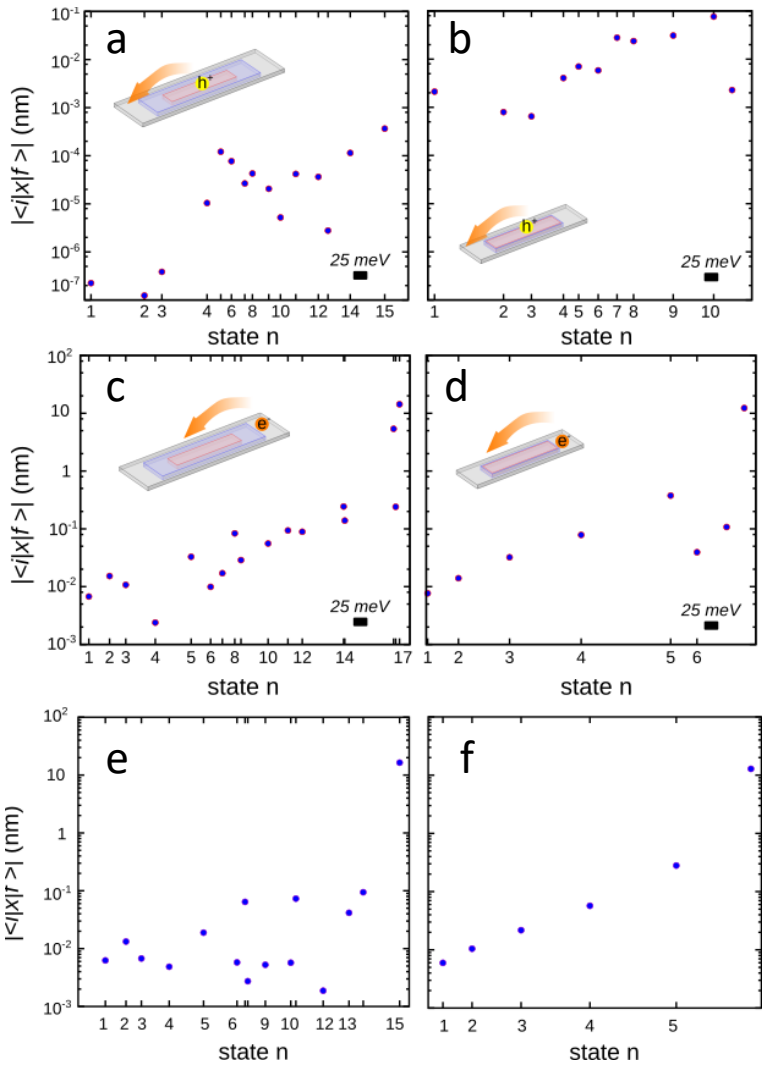

Figure S13. Logarithmic plot of dipole matrix element between: (a-b) the lowest hole state localized in the CdSe core, and all states below, (c-d) the lowest electron state localized in the CdTe crown, and all states below, (e-f) same as c-d but with narrow CdTe crown. Left and right columns refer to wide and narrow CdS barrier CBC NPLs. The structures are the same as in **Figure 5** of the main text.

3. ADDITIONAL FLUORESCENCE UPCONVERSION DATA

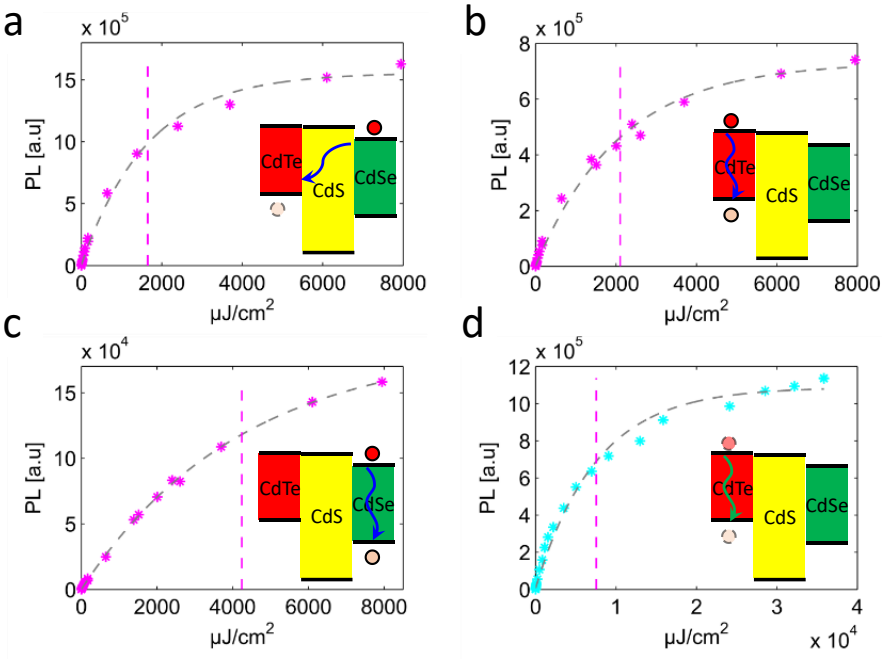

Figure S14. NPL linear saturation curves. (a-c) Linear saturation using 460 nm excitation monitored at 620, 580, 515 nm which corresponds to the indirect transition, the CdTe crown, and the CdSe core. Saturation intensities are equals to $I_{\mathrm{sat}_{620}}^{\mathrm{ex}_{460}} = 1.65\,\frac{\mathrm{mJ}}{\mathrm{cm}^2}$, $I_{\mathrm{sat}_{580}}^{\mathrm{ex}_{460}} = 2.1\,\frac{\mathrm{mJ}}{\mathrm{cm}^2}$, $I_{\mathrm{sat}_{515}}^{\mathrm{ex}_{460}} = 4.2\,\frac{\mathrm{mJ}}{\mathrm{cm}^2}$, and are plotted as dashed vertical lines. (d) Linear saturation curve of the indirect transition using 580 nm excitation, exciting the CdTe crown and the indirect transition monitored at 620 nm. $I_{\mathrm{sat}_{620}}^{\mathrm{ex}_{580}} = 7.6\,\frac{\mathrm{mJ}}{\mathrm{cm}^2}$ and is plotted as dashed vertical line.

4. REFERENCES

1. Kumagai, M.; Takagahara, T. Excitonic and Nonlinear-Optical Properties of Dielectric Quantum Well Structures. *Phys. Rev. B.* **1989**, *40*, 12359.
2. Li, Y.-H.; Walsh, A.; Chen, S.; Yin, W.-J.; Yang, J.-H.; Li, J.; Da Silva, J. L.; Gong, X. G.; Wei, S.-H. Revised *Ab Initio* Natural Band Offsets of All Group IV, II-VI, and III-V Semiconductors. *Appl. Phys. Lett.* **2009,** *94*, 212109.
3. Li, Y.-H.; Gong, X. G.; Wei, S.-H. *Ab Initio* All-Electron Calculation of Absolute Volume Deformation Potentials of IV-IV, III-V, and II-VI Semiconductors: The Chemical Trends *Phys. Rev. B* **2006,** *73*, 245206.
4. Norris, D. J.; Bawendi, M. G. Measurement and Assignment of the Size-Dependent Optical Spectrum in CdSe Quantum Dots *Phys. Rev. B* **1996,** *53*, 16338.
5. Adachi, S; *Handbook of Physical Properties of Semiconductors*, 1st Ed.; Kluwer Academic Publishers: Boston, **2004**; Vol. 3.
6. Scott, R.; Prudnikau, A. V.; Antanovich, A.; Christodoulou, S.; Riedl, T.; Bertrand, G. H.; Owschimikow, N.; Lindner, J. K.; Hens, Z.; Moreels, I.; Artemyev, M.; Woggon, U.; Achtstein, A. W. A Comparative Study Demonstrates Strong Size Tunability of Carrier–Phonon Coupling in CdSe-Based 2D and 0D Nanocrystals. *Nanoscale* **2019,** *11*, 3958-3967.
7. Pandya, R.: Chen, R. Y.; Cheminal, A.; Dufour, M.; Richter, J. M.; Thomas, T. H.; Ahmed, S.; Sadhanala, A.; Booker, E. P.; Divitini, G.; Deschler, F.; Greenham, N. C.; Ithurria, S.; A. Rao, Exciton–Phonon Interactions Govern Charge-Transfer-State Dynamics in CdSe/CdTe Two-Dimensional Colloidal Heterostructures. *J. Am. Chem. Soc.* **2018**, *140*, 14097-14111.